Experimental characterization of optical nonlocality in metal-dielectric multilayer metamaterials

Lei Sun,[1] **Fei Cheng,**[1] **Cherian J. Mathai,**[2] **Shubhra Gangopadhyay,**[2] **Jie Gao,**[1,3] **and Xiaodong Yang,**[1,*]

[1]*Department of Mechanical and Aerospace Engineering, Missouri University of Science and Technology, Rolla, Missouri 65409, USA*
[2]*Department of Electrical and Computer Engineering, University of Missouri, Columbia, Missouri 65211, USA*
[3]*gaojie@mst.edu*

[*]*yangxia@mst.edu*

Abstract: The optical nonlocality in metal-dielectric multilayer metamaterials is characterized experimentally as a function of the angle of incidence with respect to the TE-polarized incident light. The physical mechanism of the difference between the nonlocal effective permittivity and the effective-medium-theory-based effective permittivity depending on the incident angle is theoretically revealed through the analysis of the band structure, the dispersion relation, and the iso-frequency contours according to the transfer-matrix method. Such effective permittivity difference is also retrieved in the metal-dielectric multilayers based on the measured transmission and reflection spectra.

© 2014 Optical Society of America

OCIS codes: (160.3918) Metamaterials; (310.4165) Multilayer design; (260.2030) Dispersion; (310.6628) Subwavelength structures, nanostructures.

References and links

1. M. Silveirinha and N. Engheta, "Tunneling of electromagnetic energy through subwavelength channels and bends using ε-near-zero materials," Phys. Rev. Lett. **97**, 157403 (2006).
2. M. G. Silveirinha and N. Engheta, "Theory of supercoupling, squeezing wave energy, and field confinement in narrow channels and tight bends using ε near-zero metamaterials," Phys. Rev. B **76**, 245109 (2007).
3. R. Liu, Q. Cheng, T. Hand, J. J. Mock, T. J. Cui, S. A. Cummer, and D. R. Smith, "Experimental demonstration of electromagnetic tunneling through an epsilon-near-zero metamaterial at microwave frequencies," Phys. Rev. Lett. **100**, 023903 (2008).
4. B. Edwards, A. Alù, M. E. Young, M. Silveirinha, and N. Engheta, "Experimental verification of epsilon-near-zero metamaterial coupling and energy squeezing using a microwave waveguide," Phys. Rev. Lett. **100**, 033903 (2008).
5. A. Alù, M. G. Silveirinha, A. Salandrino, and N. Engheta, "Epsilon-near-zero metamaterials and electromagnetic sources: tailoring the radiation phase pattern," Phys. Rev. B **75**, 155410 (2007).
6. A. Alù and N. Engheta, "Achieving transparency with plasmonic and metamaterial coatings," Phys. Rev. E **72**, 016623 (2005).
7. J. B. Pendry, D. Schurig, and D. R. Smith, "Controlling electromagnetic fields," Science **312**, 1780–1782 (2006).
8. N. Engheta, "Circuits with light at nanoscales: optical nanocircuits inspired by metamaterials," Science **317**, 1698–1702 (2007).
9. M. Silveirinha and N. Engheta, "Transporting an image through a subwavelength hole," Phys. Rev. Lett. **102**, 103902 (2009).
10. C. Argyropoulos, P. Chen, G. D'Aguanno, N. Engheta, and A. Alù, "Boosting optical nonlinearities in ε-near-zero plasmonic channels," Phys. Rev. B **85**, 045129 (2012).

11. E. J. R. Vesseur, T. Coenen, H. Caglayan, N. Engheta, and A. Polman, "Experimental verification of $n = 0$ structures for visible light," Phys. Rev. Lett. **110**, 013902 (2013).
12. A. H. Sihvola, *Electromagnetic mixing formulas and applications* (IET, 1999).
13. J. Elser, V. A. Podolskiy, I. Salakhutdinov, and I. Avrutsky, "Nonlocal effects in effective-medium response of nanolayered metamaterials," Appl. Phys. Lett. **90**, 191109 (2007).
14. R. J. Pollard, A. Murphy, W. R. Hendren, P. R. Evans, R. Atkinson, G. A. Wurtz, A. V. Zayats, and V. A. Podolskiy, "Optical nonlocalities and additional waves in epsilon-near-zero metamaterials," Phys. Rev. Lett. **102**, 127405 (2009).
15. L. Sun, J. Gao, and X. Yang, "Giant optical nonlocality near the Dirac point in metal-dielectric multilayer metamaterials," Opt. Express **21**, 21542–21555 (2013).
16. A. A. Orlov, P. M. Voroshilov, P. A. Belov, and Y. S. Kivshar, "Engineered optical nonlocality in nanostructured metamaterials," Phys. Rev. B **84**, 045424 (2011).
17. A. V. Chebykin, A. A. Orlov, C. R. Simovski, Y. S. Kivshar, and P. A. Belov, "Nonlocal effective parameters of multilayered metal-dielectric metamaterials," Phys. Rev. B **86**, 115420 (2012).
18. A. Orlov, I. Iorsh, P. Belov, and Y. Kivshar, "Complex band structure of nanostructured metal-dielectric metamaterials," Opt. Express **21**, 1593–1598 (2013).
19. J. Gao, L. Sun, H. Deng, C. J. Mathai, S. Gangopadhyay, and X. Yang, "Experimental realization of epsilon-near-zero metamaterial stacks with metal-dielectric multilayers," Appl. Phys. Lett. **103**, 051111 (2013).
20. X. Yang, C. Hu, H. Deng, D. Rosenmann, D. A. Czaplewski, and J. Gao, "Experimental demonstration of near-infrared epsilon-near-zero multilayer metamaterial slabs," Opt. Express **21**, 23631–23639 (2013).
21. P. B. Johnson and R. W. Christy, "Optical constant of the noble metals," Phys. Rev. B **6**, 4370–4379 (1972).
22. R. Pierrea and B. Gralaka, "Appropriate truncation for photonic crystals," J. Mod. Opt. **55**, 1759–1770 (2008).
23. S. Feng, "Graphical retrieval method for orthorhombic anisotropic materials," Opt. Express **18**, 17009–17019 (2010).
24. S. Y. El-Zaizt, "Determination of the complex refractive index of a thick slab material from its spectral reflectance and transmittance at normal incidence," Optik **124**, 157–161 (2013).

1. Introduction

Recently, the epsilon-near-zero (ENZ) metamaterials, i.e., metamaterials with near-zero permittivity, emerge into the focus of the extensive exploration because of the anomalous electromagnetic features in microwave and optical frequencies. For instance, the ENZ metamaterials can squeeze and tunnel the electromagnetic energy through narrow waveguide channels [1–4] and shape the radiation wavefront [5] due to the near-zero phase variation of the electromagnetic wave inside the ENZ metamaterials. Particularly, the ENZ metamaterials can be applied in the invisible cloaking [6, 7], the design of displacement current insulation [8], and the subwavelength image transporting [9]. Besides, the ENZ metamaterials can also be used to significantly enhance the optical nonlinearities [10] and the photonic density of states [11]. In theory, the electromagnetic properties of the ENZ metamaterials are generally described by the effective medium theory (EMT) [12] for the meta-atom structures of the metamaterials being much smaller than the wavelength. However, the variation of the electromagnetic field on the scale of the meta-atom structure will in fact result in the optical nonlocality with strong spatial dispersion, thus the permittivity components will depend on both frequencies and wave vectors [13]. Recently, the optical nonlocalities in nanowire metamaterials [14] and metal-dielectric multilayer metamaterials [15–20] around the ENZ frequency have been investigated.

In this work, the optical nonlocality is theoretically and experimentally studied in the metal-dielectric multilayer metamaterials with respect to the TE-polarized incident light of different angles of incidence. The analytical description about the optical nonlocality is developed based on the transfer-matrix method. The physical mechanism of the difference between the nonlocal effective permittivity and the EMT-based effective permittivity depending on the incident angle is revealed based on the analysis of the band structure, the dispersion relation, and the iso-frequency contours (IFCs) of the metal-dielectric multilayer metamaterials. Furthermore, such effective permittivity difference as a function of the angle of incidence is also retrieved in the metal-dielectric multilayer metamaterials according to the measured transmission and reflection spectra, which agrees with the theoretical prediction.

2. Fabrication of metal-dielectric multilayer stack

Figure 1(a) illustrates the schematic of a 4-pair periodic metal-dielectric multilayer stack, composed by gold (Au) and alumina (Al_2O_3), with respect to the TE-polarized incident light. The permittivity and the thickness of the Au layer and of the Al_2O_3 layer are denoted as (ε_1, d_1) and (ε_2, d_2), respectively. The thickness of the Au layer and of the Al_2O_3 layer is individu-
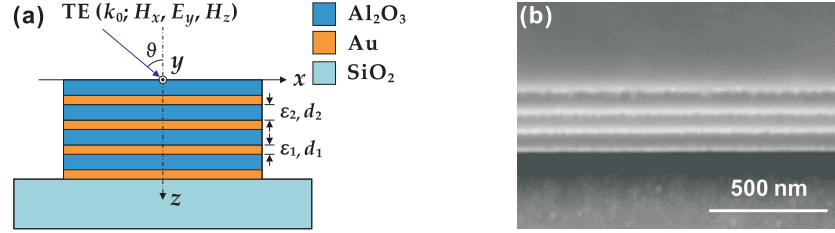

Fig. 1. (a) Schematic of the Au-Al_2O_3 multilayer stack on a quartz substrate. (b) The SEM picture of the cross section of the fabricated 4-pair Au-Al_2O_3 multilayer stack.

ally designed to be 15 nm and 70 nm. The multilayer stack is deposited on top of quartz (SiO_2) substrates with the electron-beam evaporation system, where Au is deposited at the rate of 0.4 Å/sec and Al_2O_3 is deposited at 0.2 Å/sec. Each material is individually deposited on a quartz substrate first to calibrate and optimize the deposition parameters for the electron-beam evaporation system (Kurt J. Lesker). The optical constant of each material and the film thickness are characterized with the variable angle spectroscopic ellipsometry (VASE, J. A. Woollam Co. VB400/HS-190). The VASE measurements show that the optical constant of Au matches the standard data of Johnson and Christy [21] based on the fitting from a general oscillator model. The dielectric constant of Al_2O_3 is fitted from the Cauchy dispersion relation. The VASE measured film thickness for each material also matches the thickness value for the set deposition parameters. Figure 1(b) shows the scanning electron microscope (SEM) picture of the cross section of the fabricated Au-Al_2O_3 multilayer stack, in which the focused ion beam (FIB) system (Helios Nanolab 600) is used to cut the cross section. Each deposited thin layer can be clearly seen, where the bright and the dark stripes individually correspond to the Au layers and the Al_2O_3 layers. The thickness of the deposited layers can be characterized with the VASE, and the measured averaged thickness for the Au layer and the Al_2O_3 layer is 15 ± 0.4 nm and 70 ± 1.6 nm, respectively.

3. Theoretical analysis and experimental characterization

In the long wavelength limit, the electromagnetic properties of the metal-dielectric multilayer stack can be simply described as an effective medium following a simple dispersion relation as

$$\left(k_z^2 + k_x^2\right) / \varepsilon_{\text{eff}} = k_0^2, \tag{1}$$

with respect to the TE-polarized incident light propagating in the x-z plane, as shown in Fig. 1(a). The effective permittivity ε_{eff} can be simplify determined via EMT as

$$\varepsilon_{\text{eff}}^{\text{EMT}} = \left(\varepsilon_1 d_1 + \varepsilon_2 d_2\right) / \left(d_1 + d_2\right). \tag{2}$$

Clearly, the EMT-based effective permittivity is only a function of frequency, without considering the spatial dispersion caused by the optical nonlocality. However, previous studies show that the multilayer stack possesses strong optical nonlocal effect, leading to the effective permittivity that is not only related to the frequency but also to the wave vector, especially around the ENZ

frequency. The optical nonlocality in multilayer stack can be analyzed with the transfer-matrix method, where the multilayer stack is considered as a one-dimensional photonic crystal [22,23] with the dispersion relation as

$$\cos\left(k_z(d_1+d_2)\right) = \cos(k_1 d_1)\cos(k_2 d_2) - (k_1/k_2 + k_2/k_2)/2\sin(k_1 d_1)\sin(k_2 d_2), \quad (3)$$

where $k_{1,2}^2 = \varepsilon_{1,2}k_0^2 - k_x^2$ and $k_0 = 2\pi/\lambda$ is the wave vector in free space. By substituting Eq. (1) into Eq. (3) and eliminating the wave vector k_z, the nonlocal effective permittivity including the optical nonlocality can be approximately determined as

$$\varepsilon_{\text{eff}}^{\text{nonloc}} = \frac{\arccos^2\left(\cos(k_1 d_1)\cos(k_2 d_2) - (k_1/k_2 + k_2/k_2)/2\sin(k_1 d_1)\sin(k_2 d_2)\right)}{k_0^2(d_1+d_2)^2} + \sin^2\theta. \quad (4)$$

Here the relation of $k_x/k_0 = \sin\theta$ is considered, where θ is the angle of incidence in free space. Therefore, the optical nonlocality can be indicated by the difference between the nonlocal effective permittivity determined by Eq. (4) and the EMT-based effective permittivity calculated from Eq. (2) as

$$\Delta\varepsilon_{\text{eff}} = \varepsilon_{\text{eff}}^{\text{nonloc}} - \varepsilon_{\text{eff}}^{\text{EMT}}. \quad (5)$$

According to Eq. (3), Fig. 2 displays the band structure [Figs. 2(a) and 2(b)] and the dispersion relation [Fig. 2(c)], together with the transmission [Fig. 2(d)], reflection [Fig. 2(e)] and absorption [Fig. 2(f)] spectra of the Au-Al$_2$O$_3$ multilayer stack with the optical loss of Au for different angles of incidence $\theta = 0°$ and $\theta = 50°$. It is noted that the frequency and the wave

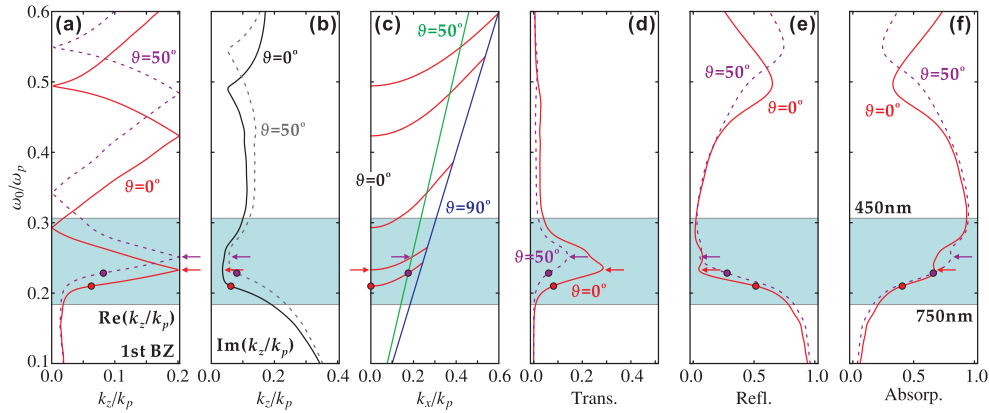Fig. 2. (a) The real part and (b) the imaginary part of the band structure of the Au-Al$_2$O$_3$ multilayer stack. (c) The dispersion relation of the Au-Al$_2$O$_3$ multilayer stack. (d) The transmission, (e) reflection, and (f) absorption spectra of the Au-Al$_2$O$_3$ multilayer stack.

vector are normalized by the plasma frequency of Au $\omega_p = 1.3666 \times 10^{16}\,$rad/s and the corresponding plasma wave vector $k_p = \omega_p/c$. The light blue region represents the wavelength range from 450 nm to 750 nm in the measurements. Figure 2(a) displays the real part of the band structure of the multilayer stack in the first Brillouin Zone (BZ). In general, the peaks in the transmission spectrum should be located at the frequencies that satisfy the Bragg's law, i.e., the points located at the center and the boundary of the first BZ. Meanwhile, the imaginary part of the band structure [Fig. 2(b)] implies the propagation loss in the multilayer stack, which is inversely proportional to the magnitude of the transmission peaks. Therefore, there is only one transmission peak for the Au-Al$_2$O$_3$ multilayer stack, corresponding to the frequency (marked by arrows) that satisfies the Bragg's law with the low propagation loss. With respect

to the variation of the angle of incidence, the optical path of each layer in the multilayer stack varies, leading to the shift of the band structure to a higher frequency for both the real part and the imaginary part, which causes the up shift of the transmission peak at the frequency from the red arrow to the purple arrow. Importantly, the frequency where $\mathrm{Re}(\varepsilon_{\mathrm{eff}}^{\mathrm{nonloc}}) = \sin^2\theta$ and $\mathrm{Re}(k_z/k_p) = \mathrm{Im}(k_z/k_0)$ also varies corresponding to the change of the band structure with respect to the angle of incidence, as marked by the dots. In the dispersion relation of Fig. 2(c), the variations of all frequencies that satisfy the Bragg's law in the real part of the band structure are plotted as a function of the wave vector $k_x \, (= k_0 \sin\theta)$, with the first branch showing the frequency where $\mathrm{Re}(\varepsilon_{\mathrm{eff}}^{\mathrm{nonloc}}) = \sin^2\theta$. Since the light lines represent different angles of incidence, the variations of the frequency where $\mathrm{Re}(\varepsilon_{\mathrm{eff}}^{\mathrm{nonloc}}) = \sin^2\theta$ and the transmission peak can be straightforwardly represented as the intersection points between the dispersion curves and the light lines at different angles of incidence, as displayed in the first branch marked with the dots and the second branch marked by the arrows, respectively. The transmission, reflection
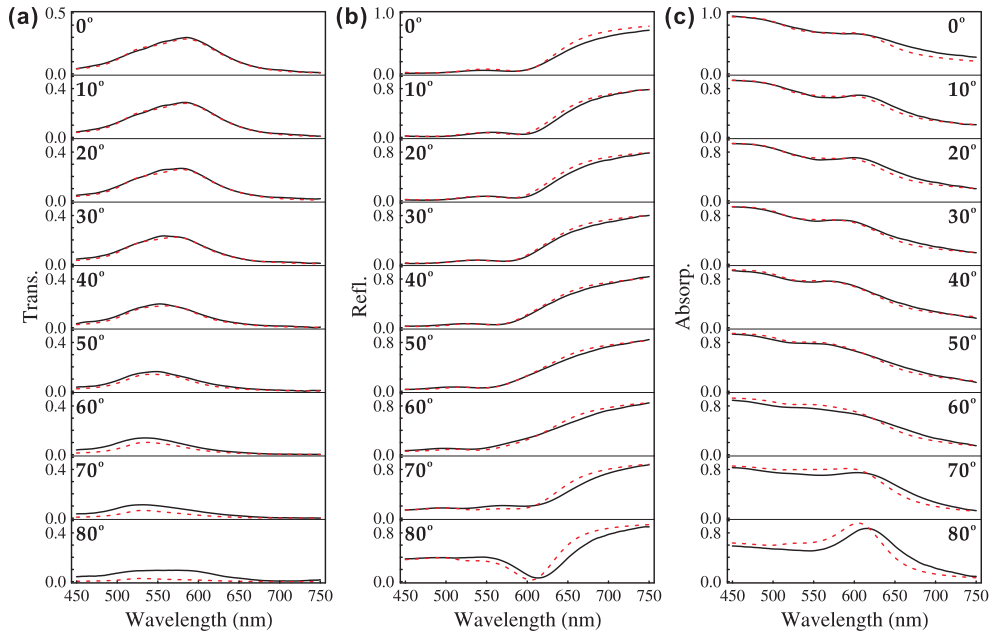

Fig. 3. (a) The transmission, (b) reflection, and (c) absorption spectra of the Au-Al$_2$O$_3$ multilayer stack in experiments (black curves) and in theory (red curves) at different angles of incidence from 10° to 80°.

and absorption spectra of the Au-Al$_2$O$_3$ multilayer stack are then measured in the wavelength range from 450 nm to 750 nm, with respect to different angles of incidence from 0° to 80° with a variation of 10°. It is shown in Fig. 3 that the experimental measurements (black-solid curves) match the theoretical predictions (red-dashed curves), including the shift of the transmission peak with respect to the variation of the angle of incidence.

In order to illustrate the optical nonlocality, Fig. 4(a) plots the difference between the nonlocal ENZ wavelength $\lambda_{\mathrm{ENZ}}^{\mathrm{nonloc}}$ calculated from Eq. (4) and the EMT-based ENZ wavelength $\lambda_{\mathrm{ENZ}}^{\mathrm{EMT}}$ according to Eq. (2) as a function of the angle of incidence. Compared to the constant EMT-based ENZ wavelength $\lambda_{\mathrm{ENZ}}^{\mathrm{EMT}} = 634.241$ nm, the difference of nonlocal ENZ wavelength varies from 22.471 nm to 21.178 nm as the angle of incidence increases from 0° to 80°. It is shown that the nonlocal ENZ wavelength of the metal-dielectric multilayer stack depends on not only the actual layer thickness but also the angle of incidence for the TE-polarized incident light. On

the other hand, Fig. 4(b) displays the difference of the effective permittivity defined in Eq. (5) as a function of the angle of incidence, at a fixed wavelength of $\lambda_{\text{ENZ}}^{\text{nonloc}}(\theta = 0^\circ) = 656.712\,\text{nm}$. Clearly, with the increase of the angle of incidence, the difference of the effective permittivity varies gradually from 0.278 to 0.263 due to the optical nonlocality.
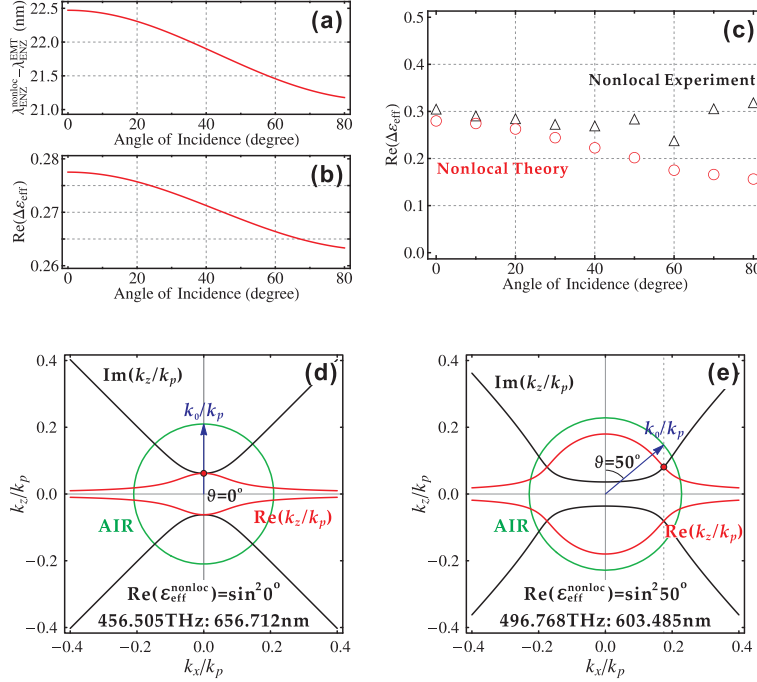

Fig. 4. (a) The difference between the nonlocal ENZ wavelength and the EMT-based ENZ wavelength as a function of the angle of incidence. (b) The real part of the effective permittivity difference at the nonlocal ENZ wavelength of $\theta = 0^\circ$ according to Eq. (5) with respect to different angles of incidence. (c) The real part of the measured effective permittivity difference (black triangles) compared to the theoretical prediction (red circles) at different angles of incidence. The IFCs at different wavelengths where $\text{Re}(\varepsilon_{\text{eff}}^{\text{nonloc}}) = \sin^2\theta$ and $\text{Re}(k_z/k_p) = \text{Im}(k_z/k_0)$ at the incident angles of (d) $\theta = 0^\circ$ and (e) $\theta = 50^\circ$.

According to the approximated approach based on incoherent interference of optical beam oscillated inside a slab, the effective propagating refractive index of the Au-Al$_2$O$_3$ multilayer stack $\tilde{n} = n + i\kappa$ (with $\tilde{n} = k_z/k_0$) can be retrieved from the measured transmission and reflection spectra as [24]

$$n = (1 + R_{as})/(1 - R_{as}) + \left(4R_{as}/((1 - R_{as})^2 - \kappa^2)\right)^{1/2}, \tag{6}$$

$$\kappa = -\lambda/(4\pi d)\ln\left(\left(T^2 - (1 - R)^2 + ((T^2 - (1 - R^2))^2 + 4T^2)^{1/2}\right)/(2T)\right), \tag{7}$$

in which d is the total thickness of the stack, and

$$R_{as} = R/(1 + (T^2 - (1 - R)^2 + ((T^2 - (1 - R^2))^2 + 4T^2)^{1/2})/2). \tag{8}$$

It has been demonstrated that the ENZ wavelength can be determined accurately for the metal-dielectric multilayer stacks according to Eqs. (6)–(8) without the phase information [19,20], due to the fact that the phase variation at the ENZ wavelength is close to zero. Moreover, the above

method will characterize the effective propagating refractive index along the direction perpendicular to the slab surface. Therefore, the frequency where $\text{Re}(k_z/k_p) = \text{Im}(k_z/k_0)$ in the band structure of the Au-Al$_2$O$_3$ multilayer stack can be determined from the measured transmission and reflection spectra at different angles of incidence. Figure 4(c) shows the difference of the effective permittivity according to Eq. (5) at the wavelength where $\text{Re}(k_z/k_p) = \text{Im}(k_z/k_0)$ with respect to the angle of incidence from $\theta = 0°$ to $\theta = 80°$. It is shown that the experimental results (black triangles) retrieved from the measured transmission and reflection spectra according to Eqs. (6)–(8) agree with the theoretical prediction (red circles) calculated from Eq. (2) and Eq. (4). The measured difference of the effective permittivity clearly shows the optical nonlocality of metal-dielectric multilayer stack compared to the EMT description. The deviations between the experimental results and the theoretical prediction at high angles of incidence are due to the fact that there is considerable difference between the measured and the calculated transmission and reflection spectra, as shown in Fig. 3. In addition, the optical phase variation in the multilayer stack is not considered in the current retrieval method.

The variation of the wavelength where $\text{Re}(k_z/k_p) = \text{Im}(k_z/k_0)$ with respect to the angle of incidence can be explained according to the analysis of the IFCs based on Eq. (3). Here two IFCs with respect to the angle of incidence $\theta = 0°$ and $\theta = 50°$ are given in Figs. 4(d) and 4(e), where the light cones are denoted as green circles and the real parts and the imaginary parts of the wave vector k_z are indicated as red curves and black curves, respectively. The point where $\text{Re}(k_z/k_p) = \text{Im}(k_z/k_0)$ is marked with red dot in the IFCs. As the angle of incidence increases from $\theta = 0°$ to $\theta = 50°$, the wave vector k_x varies from 0 to $k_0 \sin\theta$. According to the momentum conservation, the corresponding wave vector k_z varies from $0.0620227(1+\text{i})k_p$ to $0.0808913(1+\text{i})k_p$ and the wavelength shifts from $656.712\,\text{nm}$ to $603.485\,\text{nm}$.

4. Conclusions

The optical nonlocality in the metal-dielectric multilayer metamaterials for the TE-polarized incident light is theoretically studied based on the transfer-matrix method, with the analysis of the band structure, the dispersion relation, and the IFCs. The measured transmission and reflection spectra with respect to different angles of incidence for the fabricated Au-Al$_2$O$_3$ multilayer stack agree with the theoretical analysis. The difference between the nonlocal effective permittivity and the EMT-based effective permittivity depending on the angle of incidence is observed according to the retrieved refractive index results from the measured transmission and reflection spectra, which directly demonstrates the optical nonlocality in the metal-dielectric multilayer stacks.